Ultrarelativistic Heavy-Ion Collisions

Ramona Vogt

Physics Department, UC Davis, Davis, CA, USA
Nuclear Science Division, LBNL, Berkeley, CA, USA

Elsevier

Preface

This book is an extension of a course for advanced undergraduate and graduate students that I have taught at the University of California, Davis over the last ten years. It represents an attempt to gather useful information for new practitioners in the field of relativistic heavy-ion collisions in one place. As a resource for students, the text is on a rather basic level of theoretical depth. There is not a strong focus on data because the most recent data from the Relativistic Heavy Ion Collider is in a state of flux and no final conclusions have been drawn.

There are some excellent references that go beyond the scope of this book which can be used for more in-depth studies of theory. Cross sections and perturbative QCD is covered well in Halzen and Martin 'Quarks and Leptons: An Introductory Course in Modern Particle Physics', the CTEQ 'Handbook of Perturbative QCD' and, on a more phenomenological level, Perkins 'Introduction to High Energy Physics'. For more on ultraperipheral collisions, see the reviews by Baur *et al.* and Bertulani *et al.*. The review by Cleymans, Gavai and Suhonen 'Quarks And Gluons At High Temperatures And Densities' was very useful in preparation of the chapters on thermodynamics and hydrodynamics. The book 'Thermal Physics' by Kittel and Kroemer gives a good basic introduction to thermodynamics. The books 'Finite Temperature Field Theory' by Kapusta and 'Introduction to Relativistic Heavy Ion Collisions' by Csernai go further in depth in on these topics. Both Ramond 'Field Theory: A Modern Primer' and Cheng and Li 'Gauge Theory of Elementary Particle Physics' give good discussions of Grassman variables. Cheng and Li also have an excellent discussion of symmetries. A good early book on lattice gauge theory is 'Quarks,

Gluons and Lattices' by Creutz. The earlier textbook, 'Introduction to High-Energy Heavy-Ion Collisions' by Wong has an understandable section on lattice gauge theory. For finite temperature on the lattice, there are a number of very good reviews by Karsch and by Gupta.

For a snapshot of the conclusions reached from the early RHIC runs with Au+Au, d+Au and *pp* collisions at 200 GeV in the center of mass, see Volume 757 of Nuclear Physics A containing reviews by all of the first four RHIC experiments. A compendium of new data is available in the proceedings of the Quark Matter conference series, the major meeting in this field.

This book is organized into two parts. The first part covers the basic physics of heavy ion collisions with chapters on kinematics, cross sections, geometry, thermodynamics, hydrodynamics and lattice gauge theory. It includes examples in the text and exercises at the end of each chapter. The second part includes several chapters that are more like extended examples using concepts developed in the first part. The chapters on high mass thermal dileptons and quarkonium cover two high energy probes in some depth. The third discusses fragmentation and hadronization of final state particles in proton-proton collisions.

Finally, I would like to thank my colleagues at UC Davis and the students in the class that have helped make this course better. In particular I would like to mention Daniel Cebra, Mike Anderson and Brooke Haag. Roppon Picha was great help, putting all the equations in my hand-written lecture notes into LaTeX. I would like to thank Frithjof Karsch for discussions about the lattice chapter. I also thank Jean Cleymans, Vesa Ruuskanen and Bengt Friman for discussions on other sections and Joe Kapusta for useful remarks. I thanks Carl Schwarz at Elsevier for originally suggesting that I do this book and enthusiasm about the project. Last but not least I thank Jørgen and Kristina for their patience during the completion of the book.

Contents

Part I

Basics

Chapter 1

Kinematics and invariants

1.1 Introduction

Over the years, nuclear collision energies have increased from beam kinetic energies of a few MeV/nucleon on fixed targets in small university laboratories to, at present, collider energies at large laboratories with international collaborations. As the energy is increased, the relevant degrees of freedom change. At the lowest energies, the nucleus may remain intact or be broken up into light nuclear fragments. As various thresholds for particle production are reached, some of the energy of the system may go into producing new particles, such as pions or kaons. At high enough energies, the relevant degrees of freedom are expected to be quarks and gluons rather than hadrons, forming the quark-gluon plasma.

The modern era of heavy-ion collisions arrived with beam energies of 10-200 GeV/nucleon at fixed-target facilities: the Alternating Gradient Synchrotron (AGS) at Brookhaven National Laboratory (BNL) and the Super Proton Synchrotron (SPS) at the European Center for Nuclear Research (CERN). Both the AGS and the SPS accelerated protons and several types of ions onto fixed targets of heavy nuclei. While the AGS accelerated silicon, Si, and gold, Au, ions, the SPS provided oxygen, O, sulfur, S, and lead, Pb, beams as well as, more recently, indium, In. Proton-proton (pp) and proton-nucleus (pA) interactions

are used as baseline comparison measurements to distinguish true dense matter effects in nucleus-nucleus (AB) collisions from those already present in pp and pA collisions. For gold ions (nuclear mass number, A, of 197), the maximum energy at the BNL AGS was 10 GeV/nucleon while the maximum lead ion ($A = 208$) energy at the CERN SPS was 158 GeV/nucleon. Lower energy ion beams were also used to perform energy scans, down to 2 GeV/nucleon at the AGS and 20 GeV/nucleon at the SPS.

Note that the maximum energy per nucleon of the heaviest ion beam is not as high as the maximum possible proton beam energy, $E_{\max}$. The maximum energy for ions is $E_{\max}Z/A$ where Z is the proton number (nuclear charge). Protons and lighter ions can be accelerated to higher energies per nucleon, E/A, due to their larger charge-to-mass ratio, Z/A. The Z/A ratio determines the acceleration capability because while the uncharged neutrons are unaffected by the electromagnetic fields, they remain bound in the nucleus. The maximum possible center-of-mass energy for these fixed-target machines is rather low, 4.4 GeV/nucleon for Au+Au collisions at the AGS and 16.8 GeV/nucleon for Pb+Pb collisions at the SPS.

Now, two nuclear colliders take heavy-ion physics to the next level. In a collider, both collision partners, the 'projectile' and 'target' are accelerated, leading to much higher energies than those possible at fixed-target facilities. The Relativistic Heavy-Ion Collider (RHIC) at BNL and the Large Hadron Collider (LHC) at CERN produce Au+Au and Pb+Pb collisions at energies up to 200 GeV/nucleon and 5500 GeV/nucleon respectively in the center of mass. Diagrams of the RHIC and LHC accelerator complexes are shown in Figs. 1.1 and 1.2. These high energies, far above production threshold for most particles, make it possible to study the production of rare particles not accessible at lower energy facilities.

At the RHIC complex, the atoms are stripped of some of their electrons, leaving a positive charge which is accelerated by an electric field in the Tandem van de Graaff. The ions are then sent through a beam line in vacuum at 5% the velocity of light via a magnetic field. Protons are accelerated by the Linac and then sent to the Booster. Both ions and protons are further accelerated by the Booster and then

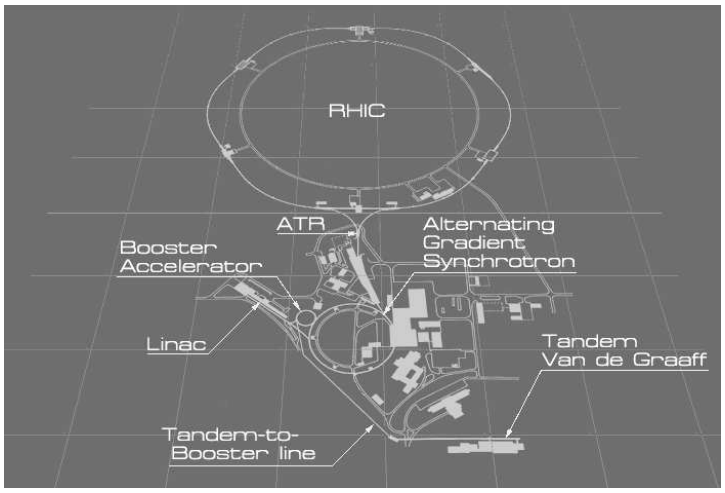

Figure 1.1: Schematic diagram of the RHIC accelerator complex [1]. Image courtesy of Brookhaven National Laboratory.

fed into the AGS where the ions are further accelerated from 37% the velocity of light to 99.7% the velocity of light. After reaching 99.7% the velocity of light, the ion beam is sent via a transfer line to the RHIC ring. A magnetic field that switches field direction sends the ions either left to travel clockwise around the ring or right to travel counterclockwise in the second ring. The ring is 2.4 miles (3.8 km) in circumference. The two oppositely-directed beams can collide at one of six interaction points. The first experiments at RHIC (STAR, PHENIX, PHOBOS and BRAHMS) occupied four of these interaction points. Together, these four experiments included 970 physicists from around the world working to build the detectors, take and analyze the data.

At the LHC, both protons and lead ions start their acceleration chain using Linacs which then feed into the Proton Synchrotron (PS) and the SPS before being transferred to the LHC rings. Note that on Fig. 1.2 there are several tangential lines lines off the PS and SPS rings (East Area on the PS and North and West Areas on the SPS) which end in fixed-target experimental areas. In addition there is a

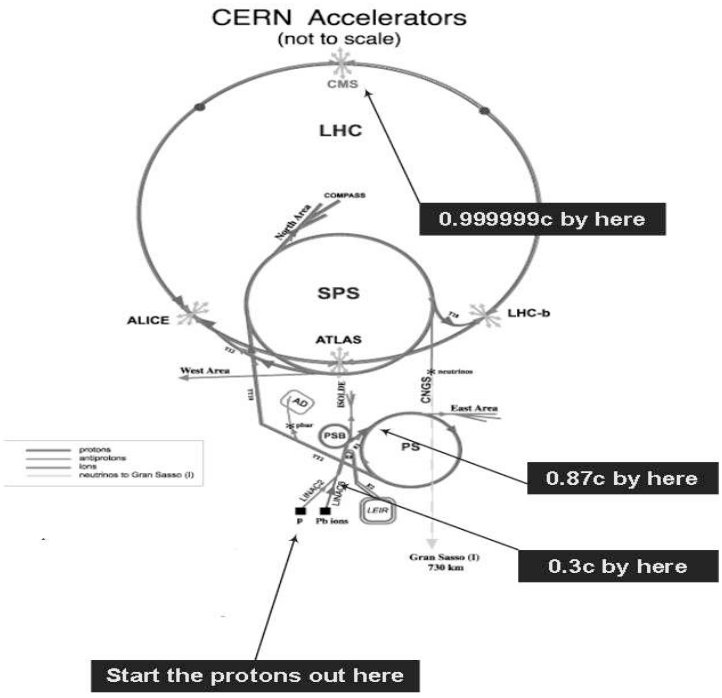

Figure 1.2: Schematic diagram of the CERN accelerators [2]. CERN copyright.

beam line from the SPS to a neutrino production area. The neutrinos are detected at the Gran Sasso laboratory in Italy, 456 miles (730 km) away. The LHC rings are 16.9 miles (27 km) in circumference. The CERN complex straddles the borders of Switzerland and France. There are four interaction points for experiments (ALICE, ATLAS, CMS and LHCb). To get an idea of the geography, ATLAS is the only detector located in Switzerland. The others are all in France. The LHC tunnel is 50-175 m underground. The varying distance below ground is due to the fact that the tunnel runs under the Jura mountain range. The ALICE experiment is dedicated to heavy-ion studies. CMS and ATLAS were mainly conceived as proton-proton experiments but CMS is also an approved heavy-ion experiment and ATLAS also has a heavy-ion group. The LHCb detector is designed to study CP violation in bottom

quark-antiquark systems. The ALICE experiment alone has more than 1000 collaborators, greater than all the RHIC experiments combined.

We will not go into detail here about the acceleration process or particle detectors but will instead concentrate on the theory behind understanding these collisions.

Here we introduce some of the important kinematic variables and notation used to describe particle interactions in heavy-ion collisions. Since heavy-ion experiments now are at energies approaching those of fundamental interactions in particle physics, it is appropriate to use relativistic kinematics and four-vector notation. The next section covers this notation while the following section deals with boost-invariant quantities.

1.2 Four-vectors and kinematic variables

We first introduce some kinematic variables that are useful to describe a particle's position and momentum. We will discuss how these variables transform under special relativity and introduce quantities invariant under Lorentz transformations.

It is useful to describe a particle's position and momentum in terms of four-vectors. In the case of position, the four-vector is represented as $\mathbf{x}^\mu$ where $\mu = 0, \cdots, 3$ and

$$\mathbf{x}^\mu = (x^0, x^1, x^2, x^3) = (ct, x, y, z) \ . \tag{1.1}$$

The zeroth coordinate is the time coordinate while $\mu = 1$, 2 and 3 are the spatial coordinates. We will use boldface type to distinguish four-vectors more explicitly here but note that this is not typically done. The right-hand side of Eq. (1.1) identifies the zeroth component of the four-vector with the time variable while the components with $\mu = 1$, 2 and 3 are the positions on the x, y and z spatial axes. The spatial four vector is often collapsed to two components with the introduction of a transverse coordinate, $x_T = \sqrt{x^2 + y^2}$, neglecting the azimuthal angle, so that

$$\mathbf{x}^\mu = (t, x_T, z) \tag{1.2}$$

where we have now taken $c = 1$, as is often done.

The momentum four-vector can be defined similarly so that

$$\mathbf{p}^\mu = (p^0, p^1, p^2, p^3) = (E/c, p_x, p_y, p_z) \tag{1.3}$$

$$= (E, p_T, p_z) \tag{1.4}$$

Note that now the zeroth component corresponds to the particle energy and $p_T = \sqrt{p_x^2 + p_y^2}$, again neglecting the azimuthal angle. We have again taken $c = 1$ between Eqs. (1.3) and (1.4).

To multiply four-vectors, we need to be able to raise and lower the indices, essentially to change a row vector to a column vector. We use the metric tensor $g_{\mu\nu}$ to raise and lower the indices where

$$g_{\mu\nu} = \begin{pmatrix} 1 & 0 & 0 & 0 \\ 0 & -1 & 0 & 0 \\ 0 & 0 & -1 & 0 \\ 0 & 0 & 0 & -1 \end{pmatrix} \quad . \tag{1.5}$$

When the metric tensor operates on a four-vector, it changes the sign of the three-vector components, $\mu = 1$, 2, 3. The four-vector with the lowered index is written as a column vector rather than a row vector so that *e.g.*,

$$\mathbf{x}_\mu = g_{\mu\nu}\mathbf{x}^\nu = \begin{pmatrix} t \\ -x_T \\ -z \end{pmatrix} \tag{1.6}$$

$$\mathbf{p}_\mu = g_{\mu\nu}\mathbf{p}^\nu = \begin{pmatrix} E \\ -p_T \\ -p_z \end{pmatrix} \quad . \tag{1.7}$$

Then, when we multiply four-vectors, we multiply a row vector with four components by a column vector with four components, resulting in a scalar. We have

$$\mathbf{a} \cdot \mathbf{b} = \mathbf{a}^\mu \mathbf{b}_\mu = g^{\mu\nu}\mathbf{a}_\mu \mathbf{b}_\nu = a^0 b^0 - \vec{a} \cdot \vec{b} \tag{1.8}$$

where $\mathbf{a}$ and $\mathbf{b}$ are any pair of four-vectors. Two cases are particularly useful in our further studies. They are the multiplication of the position

and momentum four-vectors of a particle, $\mathbf{p} \cdot \mathbf{x}$, and the multiplication of two momentum four-vectors. The first is denoted by

$$\mathbf{p} \cdot \mathbf{x} = Et - \vec{p} \cdot \vec{x} \tag{1.9}$$

while the second is

$$\mathbf{p}_1 \cdot \mathbf{p}_2 = E_1 E_2 - \vec{p}_1 \cdot \vec{p}_2 \tag{1.10}$$

which, when $1 = 2$, collapses to

$$\mathbf{p} \cdot \mathbf{p} = \mathbf{p}^2 = E^2 - |\vec{p}|^2 = m^2 \ . \tag{1.11}$$

Then, since the square of the particle mass, m, is always greater than or equal to zero, $\mathbf{p}^2 = m^2 \geq 0$ and $\mathbf{p}^2$ is a 'time-like' quantity since the zeroth components of the four-vectors dominate. If, on the other hand, the square of a four-vector is negative, $\mathbf{a}^2 < 0$, it is referred to as a 'space-like' quantity since the spatial (3-vector) contribution is largest. For example, in deep-inelastic scattering, the square of the momentum transferred from the lepton to the proton, $\mathbf{q}^2$, is negative but is usually referred to as $\mathbf{Q}^2 = -\mathbf{q}^2 \geq 0$, as we discuss later.

Figure 1.3 shows the collision of two particles at ultrarelativistic energies. The vertical axis is the time direction where the lower half plane is before the collision while the upper half plane is after the collision. The projectile comes from the left ($z < 0$) and goes off to the right. The target comes from the right ($z > 0$) and goes off to the left. The diagonal lines where $t^2 - z^2 = 0$ along the path of the 'projectile' and the 'target' define the 'light cone'. The collision occurs at $t = z = 0$. The upper part of the light cone, where $t^2 - z^2 > 0$, is the time-like region. Particle production in a real collision occurs in the upper half plane within the light cone. Outside the light cone, where $t^2 - z^2 < 0$, is the space-like region.

Most experiments are either done with either a beam on a fixed target (laboratory frame) or in a collider. We use special relativity to write the laboratory quantities in the center-of-mass frame by

$$\begin{pmatrix} E^* \\ p_z^* \end{pmatrix} = \begin{pmatrix} \gamma & -\beta\gamma \\ -\beta\gamma & \gamma \end{pmatrix} \begin{pmatrix} E \\ p_z \end{pmatrix} \tag{1.12}$$

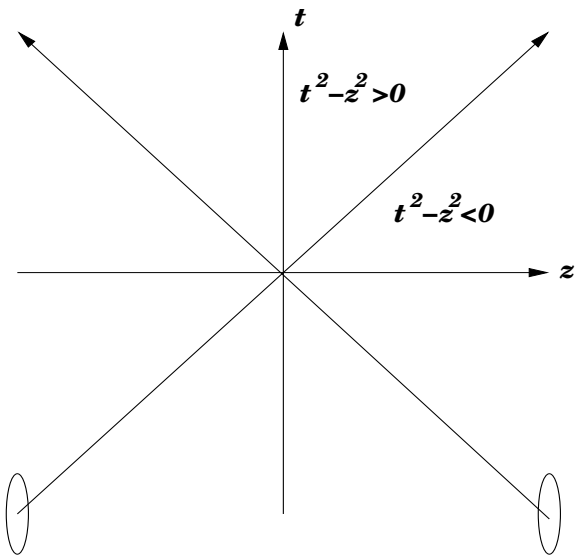

Figure 1.3: The collision axis representing one space (z) and one time dimension. The time-like ($t^2 - z^2 > 0$) and space-like ($t^2 - z^2 < 0$) regions after the collision at $t = z = 0$ are indicated.

where the variables in the new frame are 'starred'. Note that only the energy and longitudinal momentum are changed under the Lorentz transformation so that $\vec{p}_T^* = \vec{p}_T$. The velocity of the particle is denoted by β so that $\vec{\beta} = \vec{p}/E$. When transforming the projectile and target momenta from the laboratory to the center-of-mass frame, the particle has only a longitudinal velocity and we can write $\beta = p_z/E$. The gamma factor, γ, is related to the velocity by $\gamma = (1 - \beta^2)^{-1/2}$ so that, after substituting for β, we have $\gamma = E/\sqrt{E^2 - p_z^2} = E/m$ since $p_T = 0$. Then, defining β and γ as the velocity and boost factor from the laboratory frame to the center-of-mass frame, we have

$$E^* = \gamma(E - \beta p_z) \ , \tag{1.13}$$

$$p_z^* = \gamma(p_z - \beta E) \ . \tag{1.14}$$

We now define two variables that are very convenient for describing particle kinematics, the transverse mass and the rapidity. The transverse mass, m_T, is related to the difference between the squares of the

energy and longitudinal momentum,

$$m_T^2 = E^2 - p_z^2 = p_T^2 + m^2 \ . \tag{1.15}$$

It is an invariant under Lorentz transformations.

EXAMPLE: By substituting Eqs. (1.13) and (1.14) into Eq. (1.15), show that m_T^2 is an invariant.
By substitution,

$$\begin{aligned} (E^*)^2 - (p_z^*)^2 &= (\gamma(E - \beta p_z))^2 - (\gamma(\beta E - p_z))^2 \\ &= \gamma^2(E^2(1-\beta^2) - p_z^2(1-\beta^2)) \ . \end{aligned} \tag{1.16}$$

Then, using the definition of γ and β,

$$(E^*)^2 - (p_z^*)^2 = E^2 - p_z^2 \ . \tag{1.17}$$

The rapidity of a particle can also be defined in terms of its energy and longitudinal momentum, as in Eq. (1.15) above. In this case,

$$y = \frac{1}{2} \ln \frac{E + p_z}{E - p_z} \ . \tag{1.18}$$

The rapidity of the particle can be written in terms of its velocity, β, instead of the momentum and energy if we define its direction of motion to be along the z axis since $\beta = p_z/E$. Then

$$y = \frac{1}{2} \ln \frac{1 + \beta}{1 - \beta} \ . \tag{1.19}$$

We can make use of Eq. (1.18) to define the energy and longitudinal momentum in terms of the transverse mass and rapidity, using the definitions of the hyperbolic sine and cosine, $\sinh y = [\exp(y) - \exp(-y)]/2$ and $\cosh y = [\exp(y) + \exp(-y)]/2$. Then, using the definition of rapidity in Eq. (1.18), we have

$$E = m_T \cosh y \ , \tag{1.20}$$

$$p_z = m_T \sinh y \ . \tag{1.21}$$

EXAMPLE: Using Eq. (1.18), prove these equalities.

We can exponentiate the left- and right-hand sides of Eq. (1.18) to find

$$\exp(y) = \sqrt{\frac{E+p_z}{E-p_z}} \ , \qquad \exp(-y) = \sqrt{\frac{E-p_z}{E+p_z}} \ .$$

Then we form the sum and difference of the two exponentials,

$$\exp(y) + \exp(-y) = \frac{E+p_z}{\sqrt{E^2-p_z^2}} + \frac{E-p_z}{\sqrt{E^2-p_z^2}} = \frac{2E}{m_T} \ ,$$
$$\exp(y) - \exp(-y) = \frac{E+p_z}{\sqrt{E^2-p_z^2}} - \frac{E-p_z}{\sqrt{E^2-p_z^2}} = \frac{2p_z}{m_T} \ .$$

Rearranging terms and using the definitions of $\cosh y$ and $\sinh y$, we have Eqs. (1.20) and (1.21).

An advantage of rapidity over velocity is that it transforms more straightforwardly under Lorentz boosts. If y is defined as in Eq. (1.18), then, in the boosted frame,

$$y^* = \frac{1}{2}\ln\left(\frac{E^*+p_z^*}{E^*-p_z^*}\right) = y - \frac{1}{2}\ln\left(\frac{1+\beta}{1-\beta}\right) \ . \tag{1.22}$$

EXAMPLE: Prove Eq. (1.22).
Substituting the definitions of E^* and p_z^* from Eqs. (1.13) and (1.14) and rearranging terms, we have

$$\begin{aligned} y^* &= \frac{1}{2}\ln\left(\frac{E^*+p_z^*}{E^*-p_z^*}\right) = \frac{1}{2}\ln\left(\frac{\gamma(E-\beta p_z)+\gamma(p_z-\beta E)}{\gamma(E-\beta p_z)-\gamma(p_z-\beta E)}\right) \\ &= \frac{1}{2}\ln\left(\left(\frac{1-\beta}{1+\beta}\right)\left(\frac{E+p_z}{E-p_z}\right)\right) = y - \frac{1}{2}\ln\left(\frac{1+\beta}{1-\beta}\right) \ . \end{aligned}$$

We now examine two extreme cases and look at the particle rapidity. The first case is when the velocity, β, is very small, $\beta \ll 1$. Then we can expand the numerator and denominator of Eq. (1.19) to find

$$y \approx \beta \ . \tag{1.23}$$

EXAMPLE: Prove Eq. (1.23).

Using $x = 1 \pm \beta$ in Eq. (1.19), we make a Taylor expansion of $\ln x$ around $x_0 = 1$. Then

$$\ln x \approx \frac{x - x_0}{x_0} - \frac{(x - x_0)^2}{2x_0^2} + \frac{(x - x_0)^3}{3x_0^3} + \cdots \ . \tag{1.24}$$

We write Eq. (1.19) as

$$y = \frac{1}{2}[\ln(1 + \beta) - \ln(1 - \beta)] \ .$$

and substitute the values of x and x_0 ($x - x_0 = \pm\beta$) into Eq. (1.24) to find

$$\begin{aligned} y &= \frac{1}{2}[\beta - \beta^2/2 + \beta^3/3 - (\beta - \beta^2/2 - \beta^3/3)] = \frac{1}{2}[2\beta + 2\beta^3/3] \\ &\approx \beta + \mathcal{O}(\beta^3) \ . \end{aligned}$$

On the other hand, when the particle momentum is so high that the mass can be ignored, $p \gg m$, we can relate the rapidity to the pseudorapidity, η, and then to the angle of emission, θ. The pseudorapidity is often a more useful experimental measure, especially if the particles detected are not identified and their masses are thus unknown. We define the angle of particle emission relative to the z axis as $\cos\theta = p_z/p$. Then $E + p_z = \sqrt{p^2 + m^2} + p_z$ and

$$\sqrt{p^2 + m^2} = p\sqrt{1 + (m/p)^2} \approx p(1 + m^2/2p^2 + \cdots) \tag{1.25}$$

when $p \gg m$. Then

$$\begin{aligned} E + p_z &\approx p([1 + p_z/p] + m^2/2p^2) = p(1 + \cos\theta) + m^2/2p^2)) \\ &= 2p(\cos^2(\theta/2) + m^2/4p^2) \end{aligned} \tag{1.26}$$

using the definition $2\cos^2(\theta/2) = 1 + \cos\theta$. Similarly, $E - p_z = 2p(\sin^2(\theta/2) + m^2/4p^2)$ since $2\cos^2(\theta/2) = 1 - \cos\theta$. Because $p \gg m$, we can drop the second term in each equality so that

$$y \approx -\ln[\tan(\theta/2)] \equiv \eta \ . \tag{1.27}$$

It is often more convenient to use rapidity for phenomenological calculations since the mass of the desired particle is known. On the other

hand, pseudorapidity is typically used by experimentalists for reasons of convenience. As stated above, if the measured particles are unidentified, then rapidity cannot be defined as in Eq. (1.18). In addition, a typical detector or detector component covers some well-defined θ region with respect to the beam axis, making pseudorapidity a natural variable to use.

1.3 Invariants

The momentum and position of a particle are not frame invariant. However, many of the physical quantities, such as cross sections and rates, measured in experiments should be independent of the frame in which the measurement is made. Thus, for convenience, the cross sections are normally written in terms of invariants. These invariants, based on four-momenta, are used to describe interactions between particles and thus appear in calculations of the scattering cross sections. A typical two-body scattering diagram is shown in Fig. 1.4. The invariants are

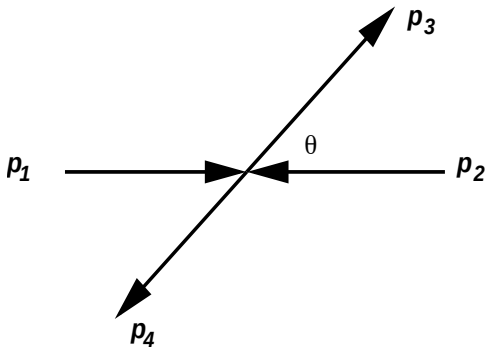

Figure 1.4: A typical $2 \rightarrow 2$ scattering diagram with particles 1 and 2 incoming while 3 and 4 are outgoing.

the squares of sums or differences of four-momenta. There are three